Korean J. Chem. Eng., 40(4), 964-974 (2023)
DOI: 10.1007/s11814-023-1380-8

pISSN: 0256-1115
eISSN: 1975-7220

Synthesis of graphene-like material derived from biomass from agricultural waste and its application in Cu (II) removal

Dessy Ariyanti*,,†, Dina Lesdantina*,**, Aprilina Purbasari*, and Yayuk Astuti*****

*Department of Chemical Engineering, Faculty of Engineering, Universitas Diponegoro, Tembalang, Semarang, Indonesia
**SDGs Center, Universitas Diponegoro, Tembalang, Semarang, Indonesia
***Departemen of Chemistry, Faculty of Science and Mathematics, Universitas Diponegoro, Tembalang, Semarang, Indonesia
(*Received 24 May 2022 • Revised 6 December 2022 • Accepted 16 December 2022*)

Abstract−The conversion of biomass from agricultural waste into valuable chemicals and materials is in the need, considering the growing demand for chemicals and materials originating from renewable resources. In this paper the feasibility of graphene-like materials preparation from biomass namely sugarcane bagasse, rice husk, coconut shell, and sawdust using modified Hummers methods was investigated. The application of the graphene-like materials resulting from the process in the Cu (II) removal via adsorption route was also studied. The characterization of samples shows the materials produced from sugarcane bagasse and coconut shells depict the pattern of reduced graphene oxide (rGO), while the materials derived from rise husk and sawdust follow the pattern of graphene. The synthesized graphene-like materials later were used as an adsorbent for Cu (II) removal. The results shows that graphene-like materials from sugarcane bagasse and coconut shells give the highest adsorption reaction kinetics with 19.76 and 19.34 mg/g, respectively, by following the second-order-pseudo model and the adsorption isotherm fitted the Langmuir model.

Keywords: Graphene, Graphene Oxide, Biomass, Hummers Method, Cu Adsorption

INTRODUCTION

The use of heavy metals in various technologies, such as in the medical, agricultural and industrial fields, has a wider impact, especially on the aquatic environment. Generally, waste that still contains heavy metals from various fields of technology will be channeled into the sea or river and cause environmental pollution. One of the heavy metals often found in water is Cu (II), where its presence can cause negative effects because it is poisonous, non-degradable and easily accumulates [1]. The effect of poisoning by metal ions depends on how long the duration of exposure is and how many doses of metal ions are absorbed [2]. This substance can enter the human body in various ways, including through plants, fish or drinking water. The maximum safe limit for Cu (II) metal in drinking water is 0.05 mg/L [3]. Heavy metals dissolved in water also have a higher tendency to be absorbed by plants. This causes heavy metals to accumulate in the roots, which are then transferred to other parts of the plant such as leaves, stems and fruit which are consumed by humans. Thus, heavy metals enter the food chain and then enter the human digestive system. Heavy metals that accumulate in the body will lead to serious diseases such as cramp, hypoglycemia, and lung and nervous system damage [4].

There are several ways to remove Cu (II) from the water body: flocculation and coagulation process, chemical precipitation, electrochemical separation, biological treatment, ion exchange, and adsorption. Of all many removal techniques available, the adsorption route is often considered as a simple, efficient, non-toxic, and yet affordable method for metal ions removal from wastewater [5,6]. Adsorption can be defined as an attachment process of atoms, ions or molecules from a gas, liquid or dissolved solid into the active site of adsorbent, thus creating a film of the adsorbate on the surface of the adsorbent [6]. The process requires materials that refer to adsorbent which requires to have large surface area and abundant of active site.

Agricultural wastes, such as sugarcane bagasse, rice husk, coconut shell, and sawdust, are biomass resources that can be raw materials for valuable chemicals and renewable energy. The carbon contained in biomass can be converted into materials that can be used as an excellent adsorbent for heavy metal removal. Graphene Oxide (GO) and reduced graphene oxide (rGO) are materials, derivative of graphene, that have unique chemical, optical and electrical properties because composed of a graphene framework and contain an oxygen functional group [7] that can act as an active site for adsorption process. GO and rGO have been widely applied in various technologies, including as biosensors, drug delivery, nanoelectronics, energy storage, supercapacitors and catalysts in waste management [8]. The synthesis of GO and rGO, which are environmentally friendly, still needs to be developed; it aims to reduce the use of toxic chemicals and the use of more natural materials. The main requirement in the synthesis of GO or rGO is that the raw materials use contain carbon. This carbon source can be obtained by utilizing waste including wood, sawdust, coconut shell, bagasse, rice husks, used tires, polymer and cellulose-based waste [9].

This study investigated the conversion of various types of biomasses to graphene-like materials (GO/rGO) using the modified Hummers method. The application of the produced materials in

†To whom correspondence should be addressed.
E-mail: dessy.ariyanti@che.undip.ac.id

adsorbing Cu (II) as a heavy metal that is often found in waters that cause contamination was also studied. The graphene-like materials based-biomass was studied in comparison with graphite-based materials treated with the same method.

MATERIALS AND METHODS

1. Materials

Sugarcane bagasse, coconut shell, sawdust, and rice husk as raw material were obtained from the local market in Semarang, Indonesia. All biomass was charred in furnace at 260 °C for 30 min at ambient environment with no specific gas condition and then ground into fine particles. Meanwhile, the chemicals such as graphite, H_2SO_4 98% (Merck), $KMnO_4$ (Merck), H_2O_2 30% (Merck), distilled water and deionized water were used without further treatment.

2. Synthesis of Graphene

The synthesis method was adapted from the modified Hummers method [7,10]. Charred biomass (5 g) was dispersed in 125 ml H_2SO_4 (98%) in an ice bath. $KMnO_4$ (15 g) was then slowly added to the mixture with continuous stirring and controlled temperature below 20 °C. The mixture was subsequently transferred to a water bath with controlled temperature 35-40 °C and stirred for 3 h. The color change during the process was observed, which commonly varies depending on the raw material used. When $KMnO_4$ is added, the whole solution will tend to be blackish purple, and over time the solution turns greenish black, which indicates that the dimanganese heptoxide compound has been formed as a result of the reaction between H_2SO_4 and $KMnO_4$.

The solution was then slowly mixed with 100 mL deionized water, as the addition of deionized water can cause bubbles and a rapid rise temperature. The temperature was maintained at 95 °C for 15 minutes. During this process the solution again changed color into light brown or dark brown for a solution made from biomass. While those made from graphite, the color will change to yellowish brown. Subsequently, additional 100 mL of deionized water was added one more time followed by 25 ml of H_2O_2 (30%), which was added slowly to remove the remaining $KMnO_4$. By this time, the sample color changed from light or dark brown to yellowish black for biomass and bright yellow for graphite. The sample was then filtered under warm conditions and repeatedly washed using distilled water until the pH became neutral. The solid sample was dried in an oven at 80 °C for 6 hours. Dried solid sample was then ultrasonically exfoliated in an ultrasonic bath (Krisbow, 50 kHz) for 30 minutes which previously dissolved in deionized water. For samples with different raw material consisting of bagasse, rice husk, coconut shell, and sawdust, respectively were labelled G-BS, G-RH, G-CS, and G-SD. While the sample synthesized from graphite was coded G-GR.

3. Characterization

The samples were characterized by XRD (SHIMADZU XRD-7000) to determine the crystal structure and Fourier transform infrared spectroscopy (FTIR) to observe the chemical bonding of the samples using PerkinElmer Spectrum IR 10.6.1. Brunauer-Emmett-Teller (BET) and Barret-Joyner-Halenda (BJH) methods (Quantachrome Instruments version 11.0) were used to estimate the specific surface area and pore volume of the sample from measurements of N_2 adsorption and desorption.

4. Adsorption Experiment Procedure

The adsorption capacity of the sample produced was observed by the effectiveness of the sample in adsorption of Cu (II) ions in the solution. The concentration of the solution used was 10 ppm with adsorbent dosage of 0.5 g/L. The adsorption process was carried out with respect to time and equilibrium achieved. The solution was taken every 15, 30, 45, 60 and 120 minutes for Cu (II) ion concentration observation using atomic absorption spectrophotometry (AAS) PinAAcle 900F. The sample was filtered to remove sediment before it was analyzed. First, the calibration was conducted for data collection used in calibration curve. Blank solutions and working solutions in various concentrations were measured at wavelength 324.75 nm to get linear regression with coefficient value of $(r)\geq 0.995$. The next step aspirated the sample into AAS-flame and then measured the absorption at a wavelength of 324.75 nm. Cu concentration of each sample was obtained and used to calculate the adsorption capacity. The adsorption capacity is calculated based on the equation [11]:

$$q_t = \frac{(C_0 - C_t) \times V_0}{w_{catalyst}} \quad (1)$$

where C_0 and C_t (mg/L) are the initial concentrations and the concentration at a given time; V_0 is the volume of the solution containing the pollutant (L); and $w_{catalyst}$ is the mass of the catalyst (g).

The Cu (II) ions concentration absorbed can be calculated using the following equation [11]:

$$\text{Removal rate} = \frac{(C_0 - C_t)}{C_0} \times 100\% \quad (2)$$

RESULTS AND DISCUSSION

1. Characterization

The conversion of graphite via modified Hummers methods produced material identified as graphene oxide based on XRD pattern analysis as shown in Fig. 1. Pristine graphite was identified by the XRD pattern in the diffraction peak of 2θ=26.54° with a distance between layers of 0.34 nm, and after conversion via modified Hummers method; the resulting material shows diffraction peaks at 2θ=10.32° and 43.9° known as graphitic plane (002) and (100), respectively, with interlayer distance of 0.88 nm [12]. The shift of the diffraction peaks indicates that the graphite has undergone a complete oxidation process and become graphene oxide. The distance between layers has changed to be wider because graphene oxide contains oxygen functional groups. This occurs as a result of multilayer carbon rotation to produce a single layer of carbon that occurs irregularly or known as turbostratic disorder [13].

Meanwhile, materials resulting from biomass from agriculture waste conversion via modified Hummers method show various diffraction peaks in the XRD pattern. The pristine charred coconut shell shows a peak at 2θ=24.5°, while the resulting materials synthesized using modified Hummers method show a peak at 2θ=23.74° with narrower peak and higher intensity. Likewise, at an angle of 43.8°, the diffraction pattern changes before and after the oxidation process. In charred coconut shell, the diffraction pattern at an

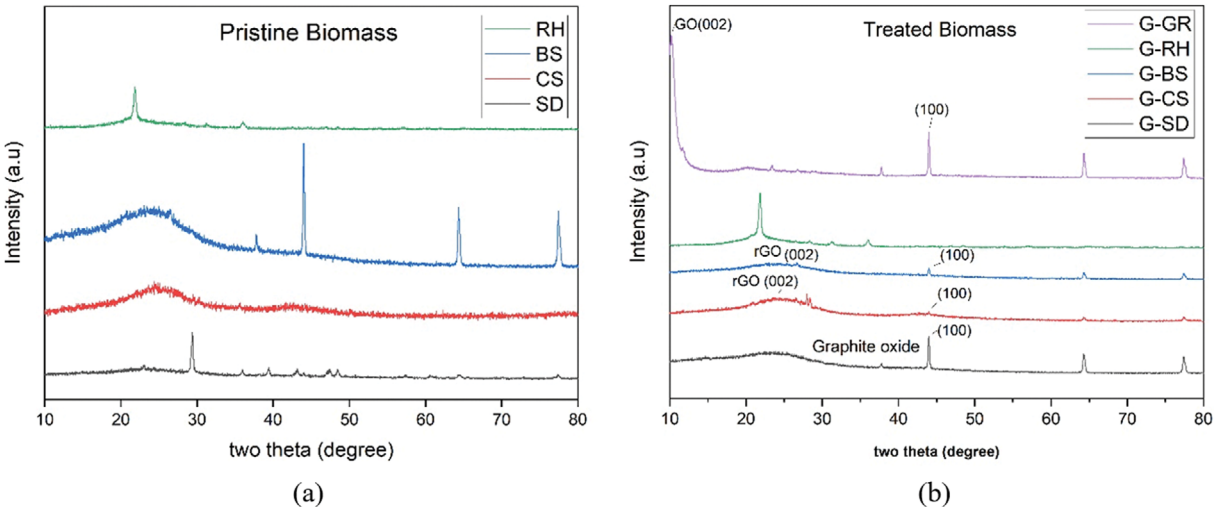

Fig. 1. XRD pattern of (a) pristine biomass and (b) samples synthesized using the modified Hummers method with raw materials of graphite (G-GR), rice husks (G-RH), bagasse (G-BS), coconut shell (G-CS), and sawdust (G-SD).

angle of 43.8° is amorphous, while the resulting product presents a narrower crystal peak. Based on Sujiono et al., two dominant peaks at 2θ=23.97° and 43.04° indicate the formation of reduced graphene oxide (rGO) [14]. Thus, the sample derived from coconut shell synthesized by the modified Hummers method was reduced graphene oxide. The claim was also reinforced by Emiru et al., which confirmed that the diffraction peak at 2θ=23.8° was reduced graphene oxide [12].

Charred rice husk shows a diffraction peak at 2θ=21.8°, and the conversion of it via modified Hummers method shows the diffraction peak at the same two theta but with higher intensity (Fig. 1). In addition, there is a peak at an angle of 2θ=36°, which represents the peak of crystalline silica (SiO_2) (111) [15]. Based on the XRD analysis result, the silica contained in the charred rice husk is suspected to remain dominant and does not show any crystal formation of graphene [15]. Carbonation or combustion at a temperature below 500 °C is not sufficient to remove the silica contained in the rice husk, which is approximately around ±35-42%, much higher than the carbon content ±6-22% [16].

The XRD pattern of materials produced from the conversion of sawdust via modified Hummers method as shown in Fig. 1, indicates the diffraction pattern of graphite oxide. In charred sawdust, the diffraction pattern shows the main peak at 2θ=29.3°, whereas the peak from the synthesized product is at 43.9° with no other major peak appearances. The structures are irregular due to random movements between adjacent layers and local configuration errors that occur in the pre-treatment process, such as the refining or heating process. Sudarsono et al. confirmed an indication of the formation of reduce graphene oxide (rGO) is the appearance of two main peaks at 23.97° and 43.04° [17]. Similar argument was also conveyed by Baqiya et al., where the characterization pattern in the single-phase rGO consists of two wide peaks in the range ~23° and ~43° [18]. The peak at 43.9° in the synthesized charred sawdust indicated that the structure formed was similar to graphite oxide [19].

The diffraction pattern of sugarcane bagasse-based material after being treated via modified Hummers method shows diffraction peaks at 2θ=26.5° and a decrease in peak intensity at 2θ=44° as presented in Fig. 1, in comparison with the charred pristine sugarcane bagasse which has peak at 2θ=44°. Li, et al. stated that the diffraction pattern at 26.5° is related to graphite or reduced graphene oxide (rGO) [20]. The formation of rGO due to raw material being only partially oxidized will produce materials at peaks at 2θ=26° [21]. The van der Waals bond between two adjacent layers, which is more dominant than the bond with the oxygen functional group on the surface, allows the formation of piles between layers again. Thus, the sample characteristics are more like pure graphite or reduced graphene oxide (rGO) [22]. Based on the shape of the wider peak in the graphitic plane (002) with an angle of 2θ=26.5° and a decrease in intensity at the peak (100) with an angle of 2θ=44°, the samples produced from sugarcane bagasse synthesis process are more likely to have characteristics similar to reduced graphene oxide [12].

FT-IR is a technique for determining the presence of functional groups contained in GO or rGO. Among all the modifications or functionalization, the presence of the oxygen functional group contained on the surface is the most significant group because it provides an active site on GO or rGO to bind with metals, organic molecules, or other heteroatoms. The existence of this functional group is always associated with the formation of new bonds in the heavy metal adsorption process, so it plays a role in the removal of heavy metals through complex formation or ion exchange. The oxygen functional groups commonly contained in GO or rGO include hydroxyl (-OH), carboxyl (-COOH), epoxy (-COC-) and carbonyl (C=O) [2].

The graphene oxide (GO) produced from graphite shows a spectrum as presented in Fig. 2, with the formation of a peak at ~1,142 cm^{-1}, which is C-O stretching of epoxy (C-O-C). While the peak in the range of ~1,623 cm^{-1} shows the presence C=C in the GO framework, which shows the un-oxidized graphite region. The C=O stretching of carboxyl is indicated by the presence of a peak at ~1,720 cm^{-1}, while in the range of ~3,402 cm^{-1} a widened peak

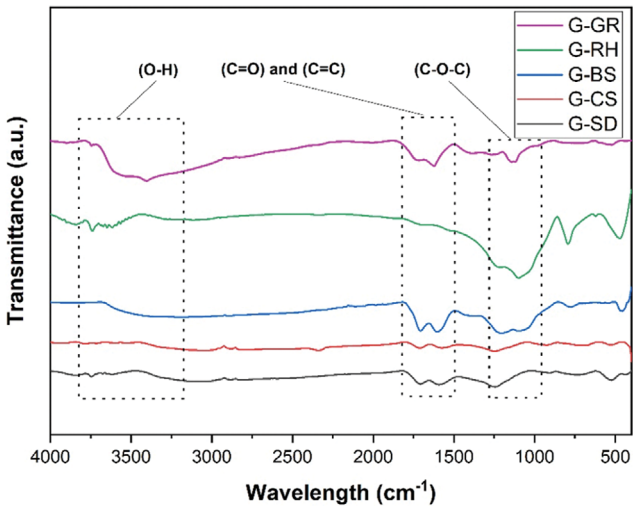

Fig. 2. FTIR spectrum of sample synthesized using the modified Hummers method with raw materials of graphite (G-GR), rice husks (G-RH), bagasse (G-BS), coconut shell (G-CS), and sawdust (G-SD).

is formed which indicates O-H stretching of hydroxyl [12].

Fig. 2 also displays the reduced graphene oxide (rGO) produced from coconut shell containing functional groups including C-O stretching with a peak of ~1,245 cm^{-1}, C=C at a peak of ~1,575 cm^{-1}, which is a graphite domain that is not oxidized; C=O is shown at the peak of ~1,715 cm^{-1}, while in the range of ~3,045 cm^{-1} [14] there is a fairly wide curve and the peak formed confirming O-H of hydroxyl. All oxygen functional groups contained in the sample with a decrease in peak intensity show the characteristics of rGO such as rGO which is made using graphite as raw material [18].

Still based on the FTIR results in Fig. 2, the sample synthesized using charred rice husk as raw material shows symmetric and asymmetric Si-O-Si groups at a wavelength of ~1,099 cm^{-1}. The resulting spectrum in the range ~1,500-3,500 cm^{-1} did not show any sharp peaks. Strong peaks were seen at ~3,616 cm^{-1} and ~3,738 cm^{-1}, which indicated the presence of hydroxyl groups [23]. Meanwhile, graphite oxide synthesized from sawdust contains functional groups including C-O stretching of epoxy (C-O-C) with a peak of ~1,243 cm^{-1}, aromatic C=C at a peak of ~1,590 cm^{-1}, C=O stretching of carboxyl shown at a peak of ~1,710 cm^{-1}, while the presence of a hydroxyl (O-H) appears at the peak of ~3,058 cm^{-1} [18]. On the other hand, the results of the FTIR analysis of the samples made from sugarcane bagasse show a widened indentation with a peak of ~3,201 cm^{-1}, indicating the presence of a hydroxyl group. The narrower peaks at ~1,705 cm^{-1} and ~1,602 cm^{-1} represent C=O and C=C. The epoxy with C-O stretching in this sample is also shown by the presence of a curve at the wavelengths of ~1,204 cm^{-1} and ~1,094 cm^{-1}. The moderate intensity of the indentation containing hydroxyl, carboxyl, carbonyl and epoxy groups in this sample occurs due to de-oxygenation, which indicates the formation of reduced graphene oxide [20].

2. The Mechanism of Biomass Conversion into Graphene-like Materials via Modified Hummers Methods

The sequence of agricultural waste biomass conversion into graphene-like materials via modified Hummers methods is represented in Fig. 3.

The reaction mechanism that occurs using modified Hummers method is as follows:

$$KMnO_4 + 3H_2SO_4 \rightarrow K^+ + MnO_3^+ + H_3O^+ + 3HSO_4^- \quad (3)$$

$$MnO_3^+ + MnO_4^- \rightarrow Mn_2O_7 \quad (4)$$

Diamanganese heptoxide (Mn_2O_7) is an active species in the oxidation process obtained through the monometallic tetra oxide MnO_4^- and MnO_3^+ reactions, as shown in the following reaction above [24]. The transformation of MnO_4^- into a more reactive form, namely Mn_2O_7, will greatly assist in the oxidation process of compounds containing carbon atoms as shown in the following reaction:

$$Mn_2O_7 + H_2SO_4 + C \rightarrow \begin{pmatrix} C\text{-}O\text{-}C \\ C\text{-}OH \\ COOH \end{pmatrix} + MnO_5 + H_2O + SO_4^- \quad (5)$$

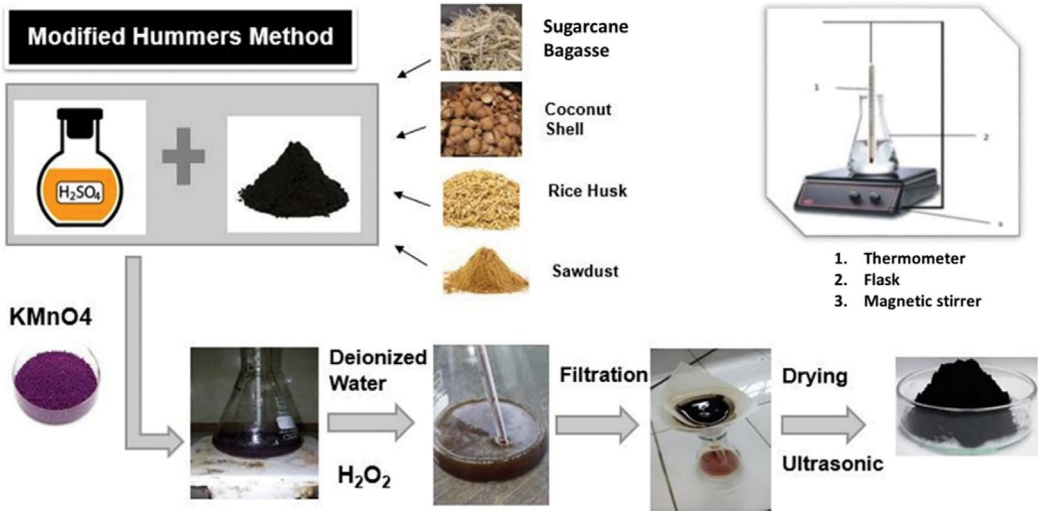

Fig. 3. Biomass synthesis stages using the modified Hummers method.

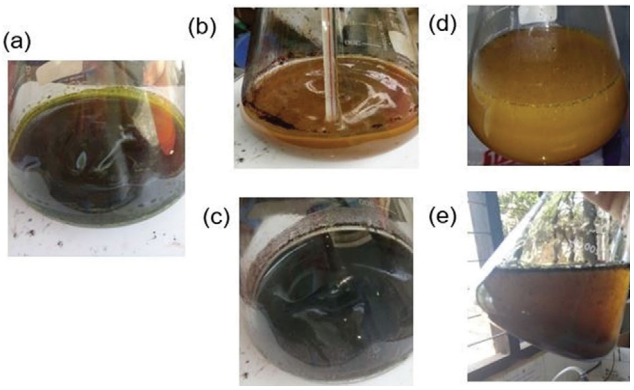

Fig. 4. Color change observation: (a) the solution turns greenish black, which indicates formed Mn_2O_7, the color change after the addition deionized water, (b) graphite, (c) biomass, and after the addition H_2O_2 (d) graphite, (e) biomass.

A color change in every sequence of the process steps was observed as depicted in Fig. 4. The addition of $KMnO_4$ turns the solution into blackish purple, and over time the solution turns greenish black, which indicates that the dimanganese heptoxide compound has been formed as a result of the reaction between H_2SO_4 and $KMnO_4$. The addition of the deionized water will again change the color of the solution into yellowish brown for graphite based material or dark brown for a solution made from biomass. Subsequently, by the addition of H_2O_2 (30%) the solution color changes from light or dark brown to yellowish black for biomass and bright yellow for graphite.

3. Adsorption Capacity

GO/rGO is known as an effective adsorbent. To investigate the effectiveness of the graphene-like materials produced from the agricultural waste biomass, the sample was used to adsorb Cu (II) ions contained in a solution. The concentration of the Cu (II) ions solution was 10 ppm with adsorbent dose of 0.5 g/L. The adsorption capacity was calculated based on Eq. (1).

As presented in Fig. 5, the adsorption process is adequately fast.

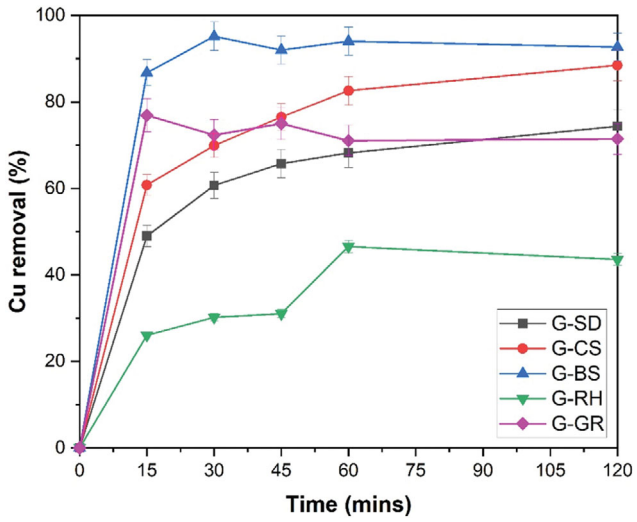

Fig. 5. Cu (II) removal from solution by using different adsorbents.

Within 15 mins, Cu (II) ions adsorb 20-90% from total concentrations. After 15 mins, the adsorption patterns vary, G-BS has slight increment, G-CS, G-RH, G-SD increase steadily, meanwhile G-GR has an unsteady pattern. However, it appears that the adsorbent's ability to remove Cu (II) ions contained in the solution tends to be more stable between 60-120 mins time frame, which indicates that the solution concentration has begun to reach equilibrium. From the graph it also can be observed that the sample synthesized from sugarcane bagasse (G-BS) shows most effective adsorption capacity in removing Cu (II) ions. This adsorbent has succeeded in removing 87% Cu (II) ions from the solution in 15 mins and removed 95% of Cu (II) ions within 30 mins.

The other adsorbent that shows good adsorption capacity is coconut shell-based graphene-like material (G-CS), which removed 61% of Cu (II) ions in the first 15 mins and eventually removed 83% Cu (II) ions during the adsorption period. Both adsorbents have an adsorption ability that is not inferior to the graphene oxide synthesized from graphite.

The characteristics of rGO synthesized from sugarcane bagasse (G-BS) and coconut shell (G-CS) indeed have a great ability in adsorbing Cu (II) ions. The existence of the oxygen functional group plays a very important role in the adsorption process because the interactions between Cu (II) ions and rGO mostly occur at the active site of oxygen atoms. The affinity of oxygen atoms to Cu (II) ions is higher than carbon skeleton [25]. The presence of oxygen functional groups, especially the carboxyl (-COOH) and hydroxyl (-OH) groups at the edge of the rGO sheet, contributes to the formation of complexes with Cu (II) ions [26]. When the adsorption process occurs, ion exchange between protons in the carboxyl and hydroxyl groups with Cu (II) ions in the solution occurs. The rGO surface which tends to be negatively charged will also cause an electrostatic attraction to the Cu (II) ions. The existence of this electrostatic attraction is the driving force in the adsorption process. The adsorption mechanism can be described as follows [27]:

$$rGO-COOH+Cu^{2+}\rightarrow rGO-COO^{-}-Cu^{2+}+H^{+} \quad (6)$$

$$(rGO-COOH)_2+Cu^{2+}\rightarrow (rGO-COO^{-})_2-Cu^{2+}+2H^{+} \quad (7)$$

$$rGO-OH+Cu^{2+}\rightarrow rGO-O^{-}-Cu^{2+}+2H^{+} \quad (8)$$

$$(rGO-OH)_2+Cu^{2+}\rightarrow (rGO-O^{-})_2-Cu^{2+}+2H^{+} \quad (9)$$

The specific surface area and pore volume of the sample were estimated from measurements of N_2 adsorption and desorption using the Brunauer-Emmett-Teller (BET) and Barret-Joyner-Hal-

Table 1. Brunauer-Emmett-Teller (BET) and Barret-Joyner-Halenda (BJH) results

Sample	Surface area (m^2/g)	Pore volume (cc/g)	Average pore radius (°A)
G-BS	15.27	0.018	38.23
G-RH	33.33	0.058	34.83
G-GR	33.98	0.141	83.21
G-CS	55.98	0.037	13.28
G-SD	24.15	0.032	26.21

enda (BJH) methods. Based on the specific surface area of a ll samples as shown in Table 1, it can be seen that the samples synthesized from coconut shell (G-CS) have the largest surface area compared to other samples. This result supports the previous finding that the G-CS has exceptionally good ability in the removal of Cu (II) ions via adsorption route.

Meanwhile, the contradictory result is shown in the G-BS material, which has smallest surface area or pore volume, yet has the best adsorption capacity. This indicates that the surface area or pore volume is not the only parameter that controls the adsorption capacity of a material. An excellent adsorption ability also can be achieved as the materials possesses large content of oxygen functional groups, which provide more active sites with higher affinity, thus can promote an easy path for the adsorbate to be adsorbed on the surface of the sample [28]. A deconvolution of the FTIR spectra was conducted to determine the amount of oxygen functional groups contained in the material based on method reported in the reference by using Fityk program [29]. The FTIR spectra regions for C-O, C=O and O-H functional groups were 1,000-1,400 cm^{-1}, 1,600-1,800 cm^{-1} and 3,000-3,500 cm^{-1}, respectively. First, all spectra were normalized by converting the transmittance value into absorbance range 0-100 and each absorbance was divided by the highest absorbance value. Then, to quantify the analysis, a deconvolution was undertaken using Fityk program, a peak fitting software, with nonlinear least squares fitting method (Gaussian function). The targeted peaks were set having fixed half width at half maximum (HWHM); to obtain the qualified fitting, the peak position was allowed to change slightly. The result of each spectra region can be seen in the

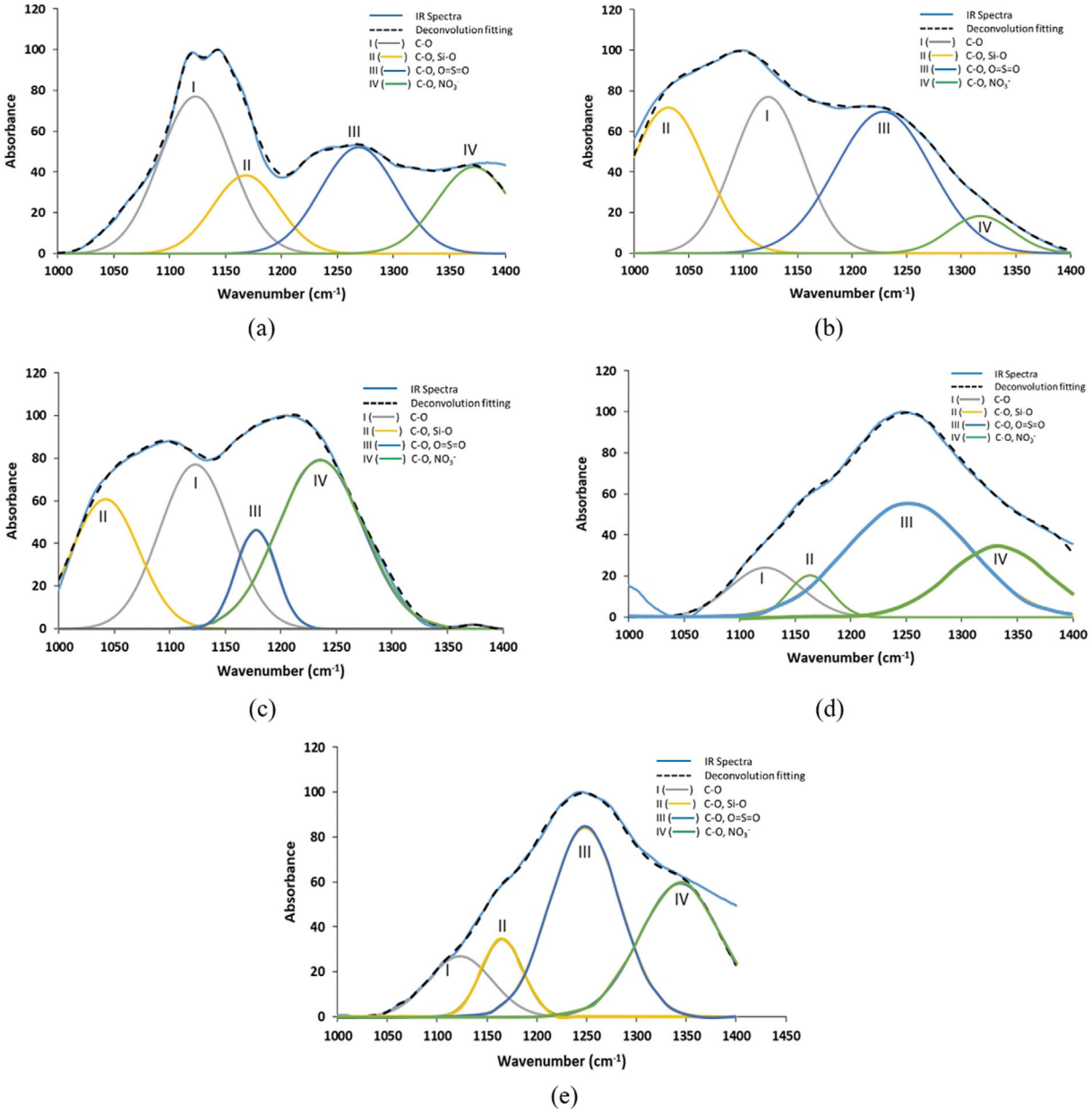

Fig. 6. Fityk result at wavenumber 1,000-1,400 cm^{-1} (a) G-GR (b) G-RH (c) G-BS (d) G-CS (e) G-SD.

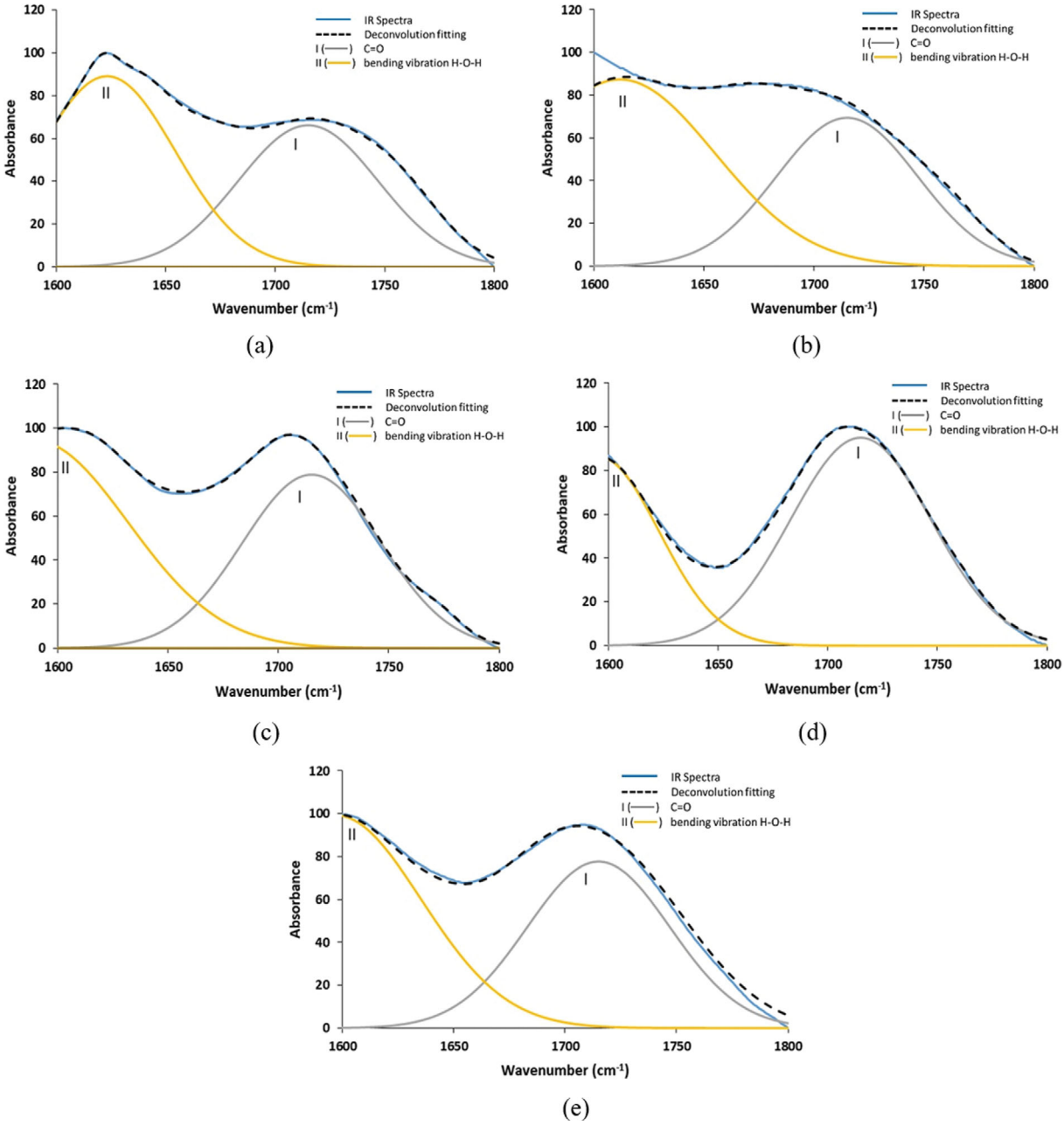

Fig. 7. Fityk result at wavenumber 1,600-1,800 cm^{-1} (a) G-GR, (b) G-RH (c) G-BS (d) G-CS (e) G-SD.

Table 2. Area ratio for functional groups C-O, C=O, O-H using Fityk program

Area calculated	G-GR	G-RH	G-BS	G-CS	G-SD
C-O (wavenumber 1,123 cm^{-1})	6,188.11	6,188.11	6,188.11	1,935.08	2,167.04
C=O (wavenumber 1,715 cm^{-1})	5,313.83	5,573.67	6,217.48	7,631.90	6,237.71
O-H (wavenumber 3,208.1 cm^{-1})	4,272.30	6,903.50	7,688.93	5,589.40	7,493.00
Total area	15,774.24	18,665.28	20,094.52	15,156.38	15,897.75

Note: *HWHM used for fityk on peak C-O, C=O=37.7° and *HWHM used for fityk on peak OH=50.4°

Figs. 6, 7 and 8.

Based on Table 2, the samples synthesized from sugarcane bagasse (G-BS) have the largest area for functional groups C-O, C=O, O-H compared to other samples supporting the excellent adsorption on G-BS Cu(II) ions removal due to the content of oxygen functional groups.

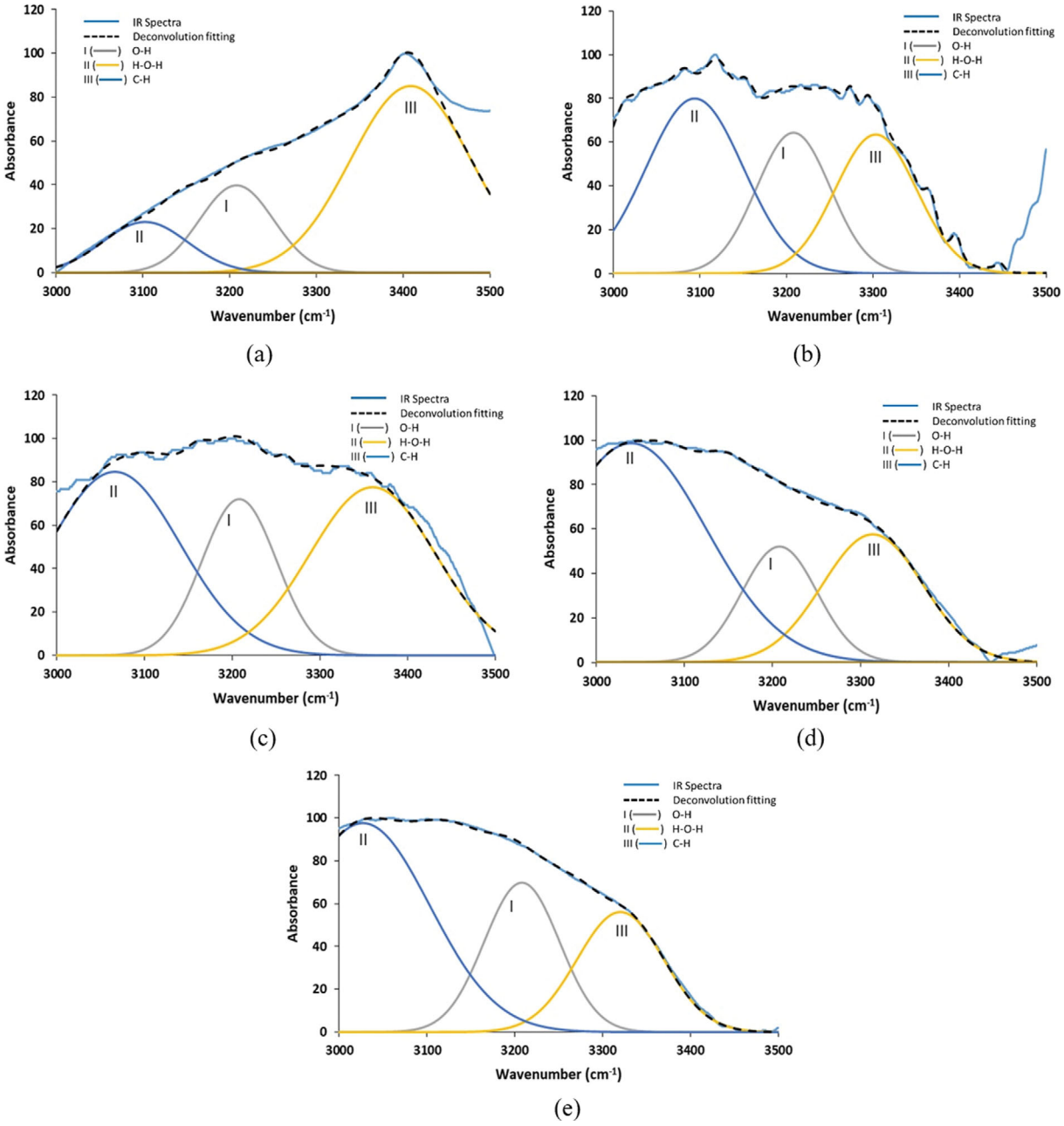

Fig. 8. Fityk result at wavenumber 3,000-3,500 cm^{-1} (a) G-GR (b) G-RH (c) G-BS (d) G-CS (e) G-SD.

3-1. Adsorption Kinetics

The kinetics of Cu metal adsorption was calculated with pseudo-first-order and pseudo-second-order models for the suitability of the research data. Model pseudo-first-order equation follows [30]:

$$\frac{dq_t}{dt} = k_1(q_e - q_t) \tag{10}$$

Equation above can be written in linearr form :

$$\ln(q_e - q_t) = \ln q_e - k_1 t \tag{11}$$

where k_1 is the rate constant of adsorption (1/min), when plotting ln ($q_e - q_t$) versus t, q_e and k_1 can be calculated.

The pseudo-second-order equation is expressed in the form [31]:

$$\frac{dq_t}{dt} = k_2(q_e - q_t)^2 \tag{12}$$

where q_e (mg/$g_{catalyst}$) is the equilibrium adsorption capacity and k_2 ($g_{catalyst}$/mg·min) is the adsorption rate constant. Take t=0 to t=t and q_t=0 to q_t=q_t as the boundary conditions, integrating the above equation to obtain the following linear form:

$$\frac{t}{q_t} = \frac{1}{k_2 q_e^2} + \frac{1}{q_e} t \tag{13}$$

the q_e and k_2 values are determined from the slope and intercept of the fitting line.

The adsorption capacity in equilibrium is presented in Table 3.

Table 3. Adsorption capacity of adsorbent in equilibrium based on experimental data

	G-BS	G-RH	G-GR	G-CS	G-SD
q_e (mg/g)	19.68	9.25	15.17	18.79	15.79

The value of the adsorption capacity obtained from the results of this work is 9.25-19.68 mg/g, with the highest capacity performed by G-BS. The highest adsorption capacity achieved in this work is almost the same as the research conducted by Mi et al., which confirms the adsorption capacity of graphene oxide to Cu is 19.1 mg/g [32].

Table 4 presents the kinetics parameters based on pseudo-first-order and pseudo-second-order models of all the graphene-like materials produced via modified Hummers method. Based on the value of the correlation coefficient (R^2), the pseudo-second order model fits the kinetics data well in comparison with the pseudo-first-order model. Likewise, the results of the calculation of equilibrium adsorption capacity (q_e) obtained from the pseudo-second-order kinetics model are closer to the equilibrium adsorption capacity calculated based on research data. The pseudo-first-order kinetics model illustrates that adsorption occurs physically (physisorption) where absorption occurs because of the weak van der Waals force without being followed by strong chemical bonds. This adsorption is also reversible, where this process can be repeated in an easy way. Meanwhile, the pseudo-second-order model describes two types of reactions that might occur. Where the two reactions can occur simultaneously or sequentially. The first reaction occurs rapidly so that equilibrium also occurs quickly. Whereas the second type of reaction runs slowly and takes longer to reach equilibrium. The pseudo-second-order model indicates that the adsorption occurs chemically (chemisorption) where the chemical bond between the adsorbate and the adsorbent is stronger; thus, chemical adsorption is a rate limiting step [2].

2-1. Adsorption Isotherm

One way to find the mechanism that might occur in the adsorption process is through the adsorption isotherm approach. This model is very useful for describing how the adsorbate is distributed between the liquid phase and the solid phase when the adsorption process reaches equilibrium [11]. To identify the Cu (II) adsorption mechanism, two different adsorption isotherm models, the Langmuir and Freundlich models, were used to match the experiment data. The Langmuir model of adsorption isotherm describes the adsorption process of a single layer (monolayer) in an adsorbent with a limited number of homogeneous active sites. This model is also based on the assumption that there are no interactions between molecules that occupy adjacent active sites. Meanwhile, the adsorption isotherm using the Freundlich model is used to explain multilayer adsorption with heterogeneous active sites [33]. The linear form of the Langmuir isotherm can be written as follows:

$$\frac{C_e}{q_e} = \frac{1}{Q^0 b} + \frac{C_e}{Q^0} \tag{14}$$

where C_e is the equilibrium concentration of adsorbate in solution (mg/L), qe is the adsorption capacity of the adsorbent at equilibrium (mg/g), Q^0 is the maximum capacity, slope which is obtained from the plot data C_e/q_e versus C_e (mg/g), while b is the Langmuir coefficient which describes the adsorption energy, intercept which is obtained from the plot C_e/q_e versus C_e (L/mg). While the Freundlich equation can be presented as follows:

$$\ln q_e = \frac{1}{nf}\ln C_e + \ln Kf \tag{15}$$

where nf is the adsorption intensity, slope is obtained from the fitted data $\ln q_e$ versus $\ln C_e$, while Kf is the Freundlich coefficient obtained from the intercept of fitted data $\ln q_e$ versus $\ln C_e$ (mg/g).

Adsorbent dosage of 0.5 g/L was reacted into Cu (II) solution

Table 4. Kinetics parameters based on pseudo-first-order and pseudo-second-order models

Sample	Pseudo-first order			Pseudo-second order		
	k_1 (g/mg mins)	q_e (mg/g)	R^2	k_2 (g/mg mins)	q_e (mg/g)	R^2
G-BS	0.070	7.39	0.774	0.457	19.76	0.999
G-RH	0.038	8.69	0.872	0.010	9.86	0.958
G-GR	0.071	6.24	0.727	0.089	15.10	0.999
G-CS	0.042	14.84	0.960	0.009	19.34	0.993
G-SD	0.040	12.06	0.948	0.011	16.26	0.994

Table 5. Isotherm parameters of Cu (II) adsorption on graphene-like materials synthesized by the modified Hummers method

Sample	Model and parameter					
	Langmuir			Freundlich		
	Q^0 (mg/g)	b (L/mg)	R^2	1/nf	K_f (mg/g)	R^2
G-BS	43.29	1.13	0.987	0.483	19.28	0.873
G-RH	15.11	0.80	0.869	0.083	10.50	0.302
G-GR	21.41	0.77	0.991	0.341	9.28	0.937
G-CS	16.05	9.00	0.995	0.123	13.40	0.812
G-SD	17.57	7.20	0.974	0.137	13.59	0.631

with various concentrations of 5, 10, 15, and 20 ppm. The parameters calculated using the Langmuir and Freundlich models are presented in Table 5.

Based on the correlation coefficient (R^2) obtained from the two models, the Langmuir model is more appropriate for the adsorption of Cu metal in all adsorbents. Data represented in Table 5 also indicated the adsorption occurs uniformly and monolayer on the adsorbent surface. Likewise, the energy required for the adsorption is the same; the active sites are spread evenly across the surface of the adsorbent and there is no interaction between adsorbates even though they are located in adjacent active sites so that one active site can only adsorb one adsorbate molecule [34]. On the other hand, the Freundlich isotherm is an empirical model that describes a heterogeneous adsorbent surface. If the 1/nf value obtained from the Freundlich equation is below 1, then the adsorption process is still profitable. This Cu metal adsorption process consists of four stages where the first step is the mass transfer of Cu metal from the bulk solution to the layer around the adsorbent. The second stage is the external diffusion of the layer surrounding the adsorbent to the outer surface of the adsorbent, while the third stage is the internal diffusion of Cu metal into the active site of the adsorbent. The last stage is the adsorption process that occurs on the active side on the inner surface of the adsorbent [2].

CONCLUSIONS

The synthesis of graphene-like material using agricultural waste biomass as raw material via modified Hummers methods was successfully carried out. Sugarcane bagasse and coconut shell as raw material show characteristics like reduced graphene oxide. This is indicated by the results of the XRD analysis that show a wider peak at 2θ=26.5° and a decrease in peak intensity at 2θ=44° for the synthesized sample using sugarcane bagasse. Meanwhile, the synthesized sample from coconut shell showed a broad peak at 2θ= 23.7°-28.18° and 43.8°. FTIR analysis of the two samples also showed the presence of oxygen functional groups, including carboxyl, hydroxyl, epoxy, and carbonyl groups. The success of this synthesis was also proven by the adsorption capacity of the two samples, which showed the best results in adsorbing Cu ions. The results show that graphene-like materials from sugarcane bagasse and coconut shells give the highest adsorption reaction kinetics with 19.76 and 19.34 mg/g, respectively. The reaction kinetics of adsorption follows a second-order-pseudo, which indicates that the adsorption is chemisorption. Likewise, the adsorption isotherm follows the Langmuir model where the adsorption that occurs is monolayer adsorption with no interaction between adsorbate molecules.

ACKNOWLEDGEMENTS

Authors acknowledged the Deputy for Strengthening Research and Development, National Research and Innovation Agency, Indonesia for the financial support No: 187-08/UN7.6.1/PP/2021.

AUTHORS CONTRIBUTION

Dessy Ariyanti contributed to the study conception and design methodology, analysis, and supervision. material preparation and data collection were performed by Dina Lesdantina. The first draft of the manuscript was written by Dina Lesdantina and all authors commented on previous versions of the manuscript. All authors read and approved the final manuscript.

DATA AVAILABILITY

The authors confirm that the data supporting the findings of this study are available within the article [and/or] its supplementary materials.

STATEMENT OF NOVELTY

Agricultural waste biomass is a prospective resource for raw materials for many valuable chemicals and products. The research was undertaken to give alternative routes of the valorization of agricultural waste biomass such as sugarcane bagasse, rice husk, coconut shell, and sawdust into graphene-like materials. By using novel modified Hummers method, the agricultural waste biomass such as coconut shell and sugarcane bagasse can be converted into rGO in the mild operating condition and hence the rGO produced can be used as an adsorbent for Cu II ions removal from wastewater up to 95% within 30 mins.

REFERENCES

1. B. Yu, Y. Zhang, A. Shukla, S. S. Shukla and K. L. Dorris, *J. Hazard. Mater.*, **80**(1-3), 33 (2000).
2. S. Z. N. Ahmad, W. N. Wan Salleh, A. F. Ismail, N. Yusof, M. Z. Mohd Yusop and F. Aziz, *Chemosphere*, **248**, 126008 (2020).
3. A. Tomczyk, Z. Sokołowska and P. Boguta, *Fuel*, **278** (2020).
4. L. Chaabane, E. Beyou, A. El Ghali and M. H. V. Baouab, *J. Hazard. Mater.*, **389**, 121839 (2020).
5. M. Pishnamazi, S. Ghasemi, A. Khosravi, A. ZabihiSahebi, A. Hasan-Zadeh and S. M. Borghei, *J. Water Process Eng.*, **42** (2021).
6. N. K. Soliman and A. F. Moustafa, *J. Mater. Res. Technol.*, **9**, 10235 (2020).
7. J. Guerrero-Contreras and F. Caballero-Briones, *Mater. Chem. Phys.*, **153**, 209 (2015).
8. Y. Seekaew, O. Arayawut, K. Timsorn and C. Wongchoosuk, *Carbon-based nanofillers and their rubber nanocomposites*, Elsevier, Inc., 259 (2019).
9. X. J. Lee, B. Y. Z. Hiew, K. C. Lai, L. Y. Lee, S. Gan, S. Thangalazhy-Gopakumar and S. Rigby, *J. Taiwan Inst. Chem. Eng.*, **98**, 163 (2019).
10. H. Muramatsu, Y. A. Kim, K.-S. Yang, R. Cruz-Silva, I. Toda, T. Yamada, M. Terrones, M. Endo, T. Hayashi and H. Saitoh, *Small*, **10** (2014).
11. Y. Li, Q. Du, T. Liu, X. Peng, J. Wang, J. Sun, Y. Wang, S. Wu, Z. Wang, Y. Xia and L. Xia, *Chem. Eng. Res. Des.*, **91**(2), 361 (2013).
12. T. F. Emiru and D. W. Ayele, *Egyptian J. Basic Appl. Sci.*, **4**(1), 74 (2017).
13. A. Allahbakhsh F. Sharif S. Mazinani and M. R. Kalaee, *Int. J. Nano Dimension*, **5**(1), 11 (2014).
14. E. H. Sujiono, Zurnansyah, D. Zabrian, M. Y. Dahlan, B. D. Amin, Samnur and J. Agus, *Heliyon*, **6**(8), e04568 (2020).

15. F. Zulti, K. Dahlan and P. Sugita, *Makara J. Sci.*, **16**(3), 163 (2012).
16. B. Armynah, Atika, Z. Djafar, W. H. Piarah and D. Tahir, *J. Phys.: Conf. Ser.*, **979** (2018).
17. W. Sudarsono, W. Y. Wong, K. S. Loh, E. H. Majlan, N. Syarif, K.-Y. Kok, R. M. Yunus and K. L. Lim, *Int. J. Energy Res.*, 1 (2019).
18. M. A. Baqiya, A. Y. Nugraheni, W. Islamiyah, A. F. Kurniawan, M. M. Ramli, S. Yamaguchi, Y. Furukawa, S. Soontaranon, E. G. R. Putra, Y. Cahyono, Risdiana and Darminto, *Adv. Powder Technol.*, **31**(5), 2072 (2020).
19. F. Fahmi, N. A. A. Dewayanti, W. Widiyastuti and H. Setyawan, *Null*, **7**(1), 1748962 (2020).
20. B. Li, X. Jin, J. Lin and Z. Chen, *J. Clean. Prod.*, **189**, 128 (2018).
21. G. Eda, J. Ball, C. Mattevi, M. Acik, L. Artiglia, G. Granozzi, Y. Chabal, T. D. Anthopoulos and M. Chhowalla, *J. Mater. Chem.*, **21**(30), 11217 (2011).
22. X. Zhang, D. C. Zhang, Y. Chen, X. Z. Sun and Y. W. Ma, *Chin. Sci. Bull.*, **57**(23), 3045 (2012).
23. P. Singh, J. Bahadur and K. Pal, *Graphene J.*, **6**, 61 (2017).
24. K. R. Koch and P. F. Krause, *J. Chem. Educ.*, **59**(11), 973 (1982).
25. Y. Cao and X. Li, *Adsorption*, **20**, 713 (2014).
26. W. Peng, H. Li, Y. Liu and S. Song, *J. Mol. Liq.*, **230**, 496 (2017).
27. W. Wu, Y. Yang and H. Zhou, *Water, Air, & Soil Pollut.*, **224**, 1372 (2013).
28. T. D. Nguyen-Phan, V. H. Pham, E. W. Shin, H. D. Pham, S. Kim, J. S. Chung, E. J. Kim and S. H. Hur, *Chem. Eng. J.*, **170**(1), 226 (2011).
29. A. Darmawan, L. Karlina, Y. Astuti, J. Motuzas, D. K. Wang and J. C. D. da Costa, *J. Non-Cryst. Solids*, **447**, 9 (2016).
30. L. Chen, J. Yang, X. Zeng, L. Zhang and W. Yuan, *Mater. Express*, **3**, 4 (2013).
31. R. Wang, K. Shi, D. Huang, J. Zhang and S. An, *Springer Nature*, **9**, 18744 (2019).
32. X. Mi, G. Huang, W. Xie, W. Wang, Y. Liu and J. Gao, *Carbon*, **50**(13), 4856 (2012).
33. A. Saravanan, T. R. Sundararaman, S. Jeevanantham, S. Karishma, P. S. Kumar and P. R. Yaashikaa, *Groundwater for Sust. Dev.*, **11**, 100460 (2020).
34. X. Wang, Y. Pei, M. Lu, X. Lu and X. Du, *J. Mater. Sci.*, **50**(5), 2113 (2015).